PNAS
www.pnas.org

Main Manuscript for:

Active strike-slip faults and an outer frontal thrust in the Himalayan foreland basin

Michael J. Duvall[a], John W.F. Waldron[a]*, Laurent Godin[b], Yani Najman[c]

[a] Department of Earth and Atmospheric Sciences, University of Alberta, Edmonton, AB, T6G2E3, Canada.
[b] Department of Geological Sciences and Geological Engineering, Queen's University, Kingston ON, K7L 3N6, Canada.
[c] Lancaster Environment Centre, Lancaster University, Lancaster, LA1 4YQ, UK.
* Corresponding author: John W.F. Waldron, Department of Earth and Atmospheric Sciences, University of Alberta, Edmonton, AB, T6G2E3, Canada. **Tel:** +1 780 492 3892.
Email: john.waldron@ualberta.ca

ORCIDs: Michael J. Duvall 0000-0001-5269-3134, John W.F. Waldron 0000-0002-1401-8848, Laurent Godin 0000-0003-1639-3550, Yani Najman 0000-0003-1286-6509

Classification

PHYSICAL SCIENCES: Earth, Atmospheric, and Planetary Sciences

Keywords

Himalaya; Thrust fault; Strike-slip fault; Foreland basin; Seismicity.

Author Contributions

Y.N. obtained access to subsurface data and L.G. initially conceived a project to investigate the role of basement ridges in the foreland basin, which was implemented by J.W.F.W. M.J.D. discovered the faults, wrote the initial draft of the paper and drafted diagrams as part of his thesis research at the University of Alberta under the supervision of J.W.F.W., who also edited the manuscript and figures for submission. All authors conducted geological field work together in Nepal, discussed the results and contributed to the science presented here.

This PDF file includes:

- Main Text

- Figures 1 to 4

Abstract

The Himalayan foreland basin formed by flexure of the Indian Plate below the advancing orogen. Motion on major thrusts within the orogen has resulted in damaging historical seismicity, whereas south of the Main Frontal Thrust (MFT), the foreland basin is typically portrayed as undeformed. Using 2D seismic reflection data from eastern Nepal, we present evidence of recent deformation propagating > 37 km south of the MFT. A system of tear faults at a high angle to the orogen is spatially localized above the Munger-Saharsa basement ridge. A blind thrust fault is interpreted in the subsurface, above the Sub-Cenozoic unconformity, bounded by two tear faults. Deformation zones beneath the Bhadrapur topographic high record an incipient tectonic wedge or triangle zone. The faults record the subsurface propagation of the Main Himalayan Thrust (MHT) into the foreland basin as a new, outer frontal thrust, and provide a modern snapshot of the development of tectonic wedges and lateral discontinuities preserved in higher thrust sheets of the Himalaya, and in ancient orogens elsewhere. We estimate a cumulative slip of ~100 m, accumulated in <0.5 Ma, over a minimum slipped area of ~780 km^2. These observations demonstrate that Himalayan ruptures may pass under the present-day trace of the MFT as blind faults inaccessible to trenching, and that paleoseismic studies may underestimate Holocene convergence.

Significance Statement

The Himalayan mountain belt results from continuing convergence between the Indian Plate and Asia. Damaging earthquakes occur on major thrust faults north of the Main Frontal Thrust (MFT). To the south, the Ganga foreland basin is typically described as undeformed. We show that active thrust and strike-slip faults, with accumulated slip up to ~100 m, pass under the trace of the MFT into the foreland basin in eastern Nepal, leading to propagation of deformation at least ~37 km into the foreland basin beneath the densely populated Ganga plain. The development of these faults at the active thrust front helps to explain structures preserved in higher thrust sheets of the Himalaya, and in ancient mountain belts elsewhere.

Main Text

Introduction

The Himalayan orogen, the Earth's highest mountain range, is a product of ongoing continent-continent collision between India and Asia (Fig. 1). The orogen is subdivided into longitudinally continuous lithotectonic domains, bounded by continent-scale faults (1, 2). The southernmost fault, the Main Frontal Thrust (MFT), separates the Himalayan foreland basin, typically regarded as undeformed, from the Sub-Himalaya, composed of thrusted and folded foreland basin sedimentary rocks (3, 4). We show that a previously unknown blind thrust and a series of strike-slip tear faults propagate southward into the Himalayan foreland basin up to 37 km south of the MFT in eastern Nepal, forming an isolated topographic feature, the Bhadrapur high that rises ~60 m above the surrounding plain (Fig. 2). We estimate slip along this incipient thrust system, and discuss the implications for the development of structure in the Himalaya and for its seismicity.

North of the MFT, the Sub-Himalaya shows lateral changes in structure along strike, resulting in variations in thrust vergence and the preservation of piggyback basins (5). Farther north, the Main Boundary Thrust (MBT) and Main Central Thrust (MCT) bound the Lesser and Greater Himalaya respectively, in which a series of along-strike culminations and depressions locally lead to the preservation of fenster and klippen (6). These major thrusts root at depth on the Main Himalayan Thrust (MHT), a crustal-scale detachment (7–10) above autochthonous Indian basement. Lateral segmentation is also evident in the episodic occurrence of seismic slip on the major thrust faults (11).

South of the MFT, the Ganga Basin (Fig. 1) is the Himalayan foreland basin (Fig. 1A) in Nepal and northern India. The basin is filled (4) by 3 to >7 km of sedimentary rock that rests unconformably on Proterozoic mobile belts, sedimentary basins, and an Archean craton, exposed along the southern edge of the basin. The stratigraphy of the basin is known from drilling and from outcrop in the Sub-Himalaya and Lesser Himalaya (12). The basin fill is divided by an Oligocene disconformity in the Sub-Himalaya (13, 14), below which a thin (>90 m) Paleogene succession is dominated by marine mudstone (15). The overlying Miocene to Quaternary rocks are fluvial deposits that filled the subsiding basin (4). This package comprises the Siwalik Group and the thinner, underlying, Dumri Formation. Seismic reflections, corresponding approximately to the lithological boundaries between the lower, middle and upper Siwalik Group, identified in the log of the Biratnagar-1 well (Fig. 2), are traced through 2D industry seismic data; the well is not deep enough to allow us to pick the Oligocene disconformity, but the deeper, angular sub-Cenozoic unconformity, representing the base of the foreland basin deposits, was traced. Locally we identified a deeper horizon marking the top of unstratified acoustic basement. Regional variations in the thickness of the Siwalik Group are controlled by a series of basement ridges (16), transverse to the orogen, of which the easternmost, Munger-Saharsa ridge, underlies the area of this study (Fig. 1). The Munger-Saharsa ridge, like other basement ridges beneath the basin, appears to be defined by NE-SW-striking faults (16) that bound Proterozoic to Paleozoic grabens beneath the foreland basin and are locally sources of earthquakes at depths >30 km (e.g. 17). Rare events well to the south of the foreland basin show normal-sense focal mechanisms (Fig. 1) but close to the MFT, and beneath the Himalaya, these faults appear to be reactivated in sinistral strike-slip (17–21).

Faults and folds within the overlying sedimentary package of the Ganga Basin are uncommon, with the result that most strata lie flat and undisturbed. The foreland basin is thus commonly presented as undeformed, despite the occurrence of earthquakes (22), river migration patterns that indicate active tectonic controls (23), and enigmatic topographic features such as the Bhadrapur high in SE Nepal (Fig. 2), which is identified as a doubly-plunging anticline in existing geologic maps (24).

Results

Using 2D seismic reflection data provided by Cairn Energy, we identify three populations of tectonic structures in eastern Nepal within a data set known as "Block 10", where faults are clustered over the Munger-Saharsa ridge (Fig. 1).

Sub-vertical strike-slip faults in the foreland basin

The first population of faults comprises six near-vertical features that crosscut most of the resolvable Cenozoic strata (Fig. 2) but do not appear to cut the sub-Cenozoic unconformity or units below. They are identified by near-vertical zones of low-amplitude, low-coherence reflectivity, interpreted as fault damage zones, across which adjacent strata are typically offset and affected by gentle to open folds. Inside the low coherence areas, several smaller near-vertical faults are typically inferred at discontinuities in the poorly coherent reflections. Folds may be differentiated as contractional or extensional, based on the upwarp or downwarp of mapped horizons relative to their regional structural level.

Correlated between profiles, the faults are traced up to 37 km, showing two main strike orientations: ~NNE-SSW and ~NNW-SSE. However, the faults show distinct bends when traced along their strike (Fig. 2) that coincide with changes between contraction and extension. We therefore interpret them as strike-slip faults. The transitions from contraction to extension in the adjacent damage zones (Fig. 2) allow us to identify bends in the fault traces as restraining or releasing, and therefore to characterize the faults as sinistral or dextral (Fig. 2).

The best-imaged releasing bend, on fault 2 shows a series of onlapping growth strata in the near-surface zone above horizon Q (Fig. 2 and Supporting Information). This indicates that strain accommodated sediment progressively, in a pull-apart basin. The maximum age of the structure is loosely estimated at ⪅0.5 Ma by interpolating from the magnetostratigraphic age (~3.5 Ma) of the near top Middle Siwalik horizon (25), assuming a constant sedimentation rate.

Steep normal faults below the foreland basin

A second set of faults is interpreted below the foreland basin fill, with apparent normal offset (Fig. 3A). These are interpreted as bounding a Gondwanan half-graben due to their proximity with the Purnea Basin (26). When correlated between lines, these basement-cutting faults strike SW-NE, sub-parallel to the faults that bound the basement ridges, a different orientation from the foreland basin faults. The basement faults appear truncated at the sub-Cenozoic unconformity. Because of this, we infer that they formed prior to foreland basin development. The limited data from earthquakes south of the Ganga Basin (17) suggest present-day dip-slip reactivation of these faults. However, strong earthquakes at depths >40 km on the trend of the Munger-Saharsa Ridge (Fig. 1), beneath the northern Ganga Basin and the Himalaya, indicate sinistral strike-slip reactivation (17–20).

Dipping reverse faults and folds within the foreland basin

The third set of structures comprises inclined reverse faults and folds coinciding with the Bhadrapur topographic high (Fig. 2), where we identify a region of shortening deformation extending ~13 km along strike, and ~2 km wide in N-S extent (Fig 3B). Three main deformed zones are imaged. The southern zones (E and F; Fig 3B) represent fold axial surfaces, separating domains of reflections with different dip. The northern deformed zone (G) additionally displays small reverse-sense offsets. The lateral terminations of these zones coincide with steep faults 1 and 2, that show opposing senses of strike slip, indicating southward relative displacement of the deformed block.

The deformation zones do not appear to offset the sub-Cenozoic unconformity or the rocks below; steep faults (set 2) in the underlying units locally coincide with the deformation zones (e.g. Fig. 3A), but show contrasting strike when correlated between profiles. The deformation zones are therefore interpreted as detached from basement above a thrust décollement near the base of the Cenozoic section.

Deformation zones E and F are interpreted as fault-bend folds, developed above changes in the dip of the underlying décollement. The northern zone G is either a reverse fault or a small-scale asymmetric fault-propagation fold; the resolution of the seismic data is insufficient to distinguish these possibilities. The curvature of these folds in map view (Fig. 2) accounts for gentle anticlines seen on line C (Fig. 3A), where the fault-bend folds E and F obliquely cut the seismic profile. Based on the changes in dip observed at the folds, the basal thrust shows a maximum dip of ~5° S (Fig. 3). The fault plane is inferred to be part of a décollement surface within or below the lower Siwalik Group. Deformation zones E-G extend toward the surface, although the individual deformation zones become more diffuse, and their total amplitude decreases. This is consistent with progressive development of the structural high during an interplay of sedimentation and erosion in its development. These structures are likely responsible for the present-day Bhadrapur high which rises ~60 m above the surrounding Ganga plain. Overall, the geometry indicates an incipient tectonic wedge or triangle zone linked to the blind basal décollement (Fig. 3B), similar to more developed triangle zones found at orogenic thrust fronts in older orogens (e.g. 27, 28).

There is no evidence that the basal décollement crosscuts the strike-slip faults in the foreland basin, and the strike-slip faults do not appear to extend deeper than the décollement. This leads us to interpret the observed geometry as a system of blocks bounded laterally by tear faults (29), similar to prominent tear faults confined to individual thrust sheets in other thrust belts (30, 31).

These blocks accommodated differential southward displacement, possibly representing an incipient salient in the thrust front. The basal décollement is therefore a subsurface extension of the MHT into the foreland basin, an outer frontal thrust. The segment beneath the Bhadrapur High is distinguished here as the Bhadrapur Thrust.

Discussion

Spatial localization of faults over basement ridges

The system of faults observed in our study spatially overlies the Munger-Saharsa Ridge (32). The Himalayan foreland basin overlies at least eight comparable structural highs, and strike-slip motion is associated with at least three (22, 33). NE-SW tear faults spatially associated with both the Delhi-Haridwar and the Munger-Saharsa ridge (Fig. 1) have been interpreted to result from basement fault reactivation (21, 34), as have comparable faults farther west (33). Modelling experiments (21) have shown that oblique basement normal faults may be reactivated in strike-slip during convergent deformation.

However, our seismic interpretation indicates that the tear and thrust faults in Block 10 are largely independent of basement structures. Although these fault systems are located preferentially above basement ridges, and are in many cases located above basement faults (Fig. 1), their strikes are different, and the basement faults do not appear to be associated with discrete offsets of the sub-Cenozoic unconformity. We suggest that the basement structures provide indirect control on the nucleation of tear and thrust faults in the overlying foreland basin, by providing small initial offsets, or by controlling factors such as the topography of the sub-Cenozoic unconformity, the thickness of the overlying sedimentary basin, or the distribution of facies that affect basal friction or fluid pressure in the thrust wedge. These parameters have been shown to control thrust propagation and transfer-zone development in analogue models (35).

Slip estimates

Independent estimates of slip are here calculated from two deformed zones, based on the assumption that the volume of rock displaced above or below its regional elevation is equal to the volume in the subsurface lost or gained through shortening or extension. This assumption may not be strictly valid, as recent sediments may undergo significant lateral compaction during thrusting (36), resulting in volume loss; which would lead to an underestimate of slip.

The first estimate uses line-length and area balancing to measure uplift and therefore constrain shortening in the subsurface fault-bend fold system below the Bhadrapur high (Fig. 4A). Area balancing yields an estimate of 90 m of southward slip, whereas bed-length balancing yields estimates of 97 – 112 m, depending on the seismic profile used.

The second estimate uses the volume of accommodation in a pull-apart basin on fault 2 to solve for slip (Fig. 4B, C). Estimates based on the pull-apart basin vary depending on the subsurface shape of the deformed volume; the geometry shown in Fig. 4B yields an estimate of 82 m.

Both methods are subject to significant uncertainties, but give an order-of-magnitude estimate of possible slip on the outer frontal thrust since its initiation. The slightly lower value obtained from the pull-apart basin, when compared with the frontal folds, suggests that the pull-apart basin records differential motion between two blocks that have both been displaced southward.

Implications for Himalayan structure and seismicity

The data presented show that Himalayan deformation propagates along a near-horizontal décollement that extends ~37 km south of the MFT; this propagation distance is several orders of magnitude greater than the inferred slip, much farther than blind thrusts previously interpreted (37) south of the MFT. The tear faults deform strata to the top of the seismic data, showing that they have been active in the Quaternary. Modern topographic highs above the thrust fault (Fig. 2) and the restraining bend of tear fault 2 (Fig. 4C) suggest that they are actively developing, despite the absence of historical earthquakes on the faults. These faults therefore provide a present-day snapshot of the early development of tear faults and tectonic wedges, structures developed in higher thrust sheets of the Himalaya (5) and in ancient orogens elsewhere (e.g. 27, 28, 31).

The observed system of tear faults appears to accommodate differential slip along strike, segmenting the upper layers of the foreland basin into blocks that have advanced different distances into the foreland basin. We therefore view the Block 10 area (Fig. 1) as an incipient salient. Along-strike segmentation in the structure (6, 16) and seismicity (11) farther north in the Himalaya may have originated from tear faults or lateral ramps developed over basement ridges with similar geometries (6).

Our results have implications for seismicity and seismic hazard. Figure 1B summarizes the record of seismicity in the region of Block 10 and the section of the Himalaya to the north. Although significant earthquake damage has occurred in the Ganga alluvial plain, most seismicity has been attributed either to slip on the MFT or faults to the north (Fig. 1). Minor earthquakes to the south of the MFT have been inferred to originate in the Indian crustal units below the Himalayan foreland basin (38). Our results show that Himalayan thrust ruptures may pass under the surface trace of the MFT as blind faults inaccessible to trenching. Because interseismic strain is negligible for a distance ~100 km north of the MFT(e.g. 39), movement on these ruptures must have occurred in response to great Himalayan earthquakes with recurrence intervals of 500-1000 yr. Paleoseismic studies around the outcrop trace of the MFT may therefore underestimate Holocene convergence.

Bilham (11) has tabulated current slip potential of segments of the Himalaya, and shows a potential slip >10 m for the segment immediately north of Block 10. Trenched fault planes along the MFT of eastern Nepal suggest the most recent significant earthquake occurred between 1146 and 1256 AD, and reflected ~11 m of slip (40). Given that modern convergence rates in Eastern Nepal are ~ 17 mm/year, this segment of the orogen is overdue for a large earthquake (11, 40).

We estimate the largest slipped segment of the outer frontal thrust, the Bhadrapur Thrust, (diagonal shading in Fig. 2) at ~780 km^2, south of its subsurface branch line with the MFT (dipping ~30°N). Slip on this area of décollement has the potential to significantly add to the energy release associated with a seismic event that passes under the surface trace of the MFT (11). However, slip at the shallow depths (<4 km) of the thrust may be accommodated by creep or episodic tremor and slip (41). Nonetheless, the high population density and the poorly consolidated surficial sediments in the Ganga Basin increase the hazard of even a moderate earthquake.

Materials and Methods

Seismic interpretation

Two-dimensional (2D) migrated seismic reflection data were used to assess basin geometry and identify faults within the foreland basin succession (Fig. 2, 3). Seismic imaging is generally good in the upper, stratified section representing sedimentary rocks of the Ganga Basin, but poor in deeper parts of the section (interpreted as basement), where the occurrence of “smiles” suggests incorrect migration velocities. Local steeply dipping artifacts in the upper section, mainly diffraction effects from faults and basement features, were easily distinguished where they cross-cut the dominant subhorizontal reflections from the sedimentary strata (see Supplementary Information).

Four regional horizons were interpreted to characterize the geometry of the foreland basin. These are, from bottom to top:

- Top of acoustic basement, interpreted as the boundary between Archean to Proterozoic plutonic and metamorphic rocks (blue horizon)
- Sub-Cenozoic unconformity, representing the top of stratified Mesoproterozoic to Paleocene strata representing the sedimentary cover of the Indian craton (pink horizon). In locations without these strata, the Sub-Cenozoic unconformity is interpreted to coincide with the acoustic basement
- Near-top lower Siwalik (orange) horizon, a strong negative reflector that lies close to the boundary between the lower and middle Siwalik Group, at ~11.05-8 Ma (25, 42)
- Near-top middle Siwalik (green) horizon, a strong positive reflector close to the boundary between sandstone-dominated middle Siwalik Group and the conglomerate-dominated upper Siwalik Group and overlying Quaternary alluvium at ~4.6-3 Ma (25).

The horizons were tied to a nearby well (Biratnagar-1; Fig. 1), and depth-converted using a time-depth relationship established using the checkshot data from the well (as sonic logs were not available). Faults were identified by noting areas with vertical separation of reflections and low signal coherence. Most faults are associated with wide (150-3000 m) zones of low reflection coherence, interpreted as damage zones.

To estimate slip, we follow a 2D balancing method from Suppe (43), (Fig. 4A) but work, where necessary, with 3D volumes instead of 2D areas (Fig. 4B, C).

Uplift beneath the Bhadrapur High

The kink construction simplifies the geometry of cylindrically deformed rocks, creating a series of straight-line segments bisected by axial surfaces (Fig. 4A). The methodology provides a satisfactory approximation even for rounded folds if they have parallel (class 1A of Ramsay (44)) geometry, because any smooth parallel fold can be approximated by a series of straight line segments. The kink construction was used to inform the placement of interpreted thrust ramps and branch points on the N-S seismic sections (Fig. 3B), because stratigraphic surfaces show more coherent reflectivity than the faults themselves. Slip is estimated by comparing the length of the deformed beds to strata that are undeformed and follow regional dip. Kink constructions were made for two profiles near the centre of the fold, to estimate the maximum slip. For the fault-bend fold resulting from the subsurface thrust, calculated slip was 97 m and 112 m, corresponding to a shortening of ~4% in both cases. An alternative construction uses the area under the folded surface (area of structural relief A_{sr}) as a proxy for the volume of deformation (Fig. 4A). For this method, an estimate of the depth to detachment is required, but it is not necessary to assume conservation of bed lengths. The area under the folded surface, below the regionally interpreted near-top-Middle-Siwalik horizon A_{sr} = 121,100 m^2 (Fig. 4A). We estimate the depth below this, to the detachment, to be 1350 m resulting in an estimated slip of 90 m, similar to the estimate of 97 m obtained by comparing line lengths on the same seismic line.

Strike slip estimated from pull-apart basin subsidence

For any 3D area that undergoes shortening or extension, the volume between the original elevation of a horizon and its deformed elevation (volume of structural relief V_{sr}) is equivalent to the volume of shortening or extension (Fig. 4) (43), provided neither volume is affected by erosion or compaction. In a plane-strain situation (such as a linear rift or a straight thrust belt), these volumes are represented by areas in cross-sections drawn parallel to the transport direction (Fig. 4A). However, in a situation such as a pull-apart basin, plane strain cannot be assumed and the methodology must be applied in 3D (Fig. 4B).

To calculate the volume of accommodation (equivalent to V_{sr}), we worked with two 2D profiles that imaged a releasing and restraining bend of the same fault; one strike profile and one dip profile (Fig. 4C). To avoid the effects of erosion at the restraining bend, we worked only with accommodation in the releasing bend. First, we identified a reflection that marked the base of accommodation. This was picked as the deepest continuous reflection that had onlapping reflections above, and no divergence of reflections below. The regional 'original' elevation of the bed was then determined from adjacent lines with flat, layer-cake stratigraphy. We then calculated how much the base of accommodation pick had subsided from its regional level along the two perpendicular seismic profiles.

We then used these two perpendicular profiles to interpolate contours (Fig. 4C) and estimate a total volume of subsidence over the inferred area affected by extension $V_{sr} = 1.9 \times 10^8$ m^3

From the volume of structural relief, shortening is estimated, for the geometry shown in Fig. 4B, from:

$$V_{sr} = swD/2$$

where *s* is the slip; *w* is the width of the deformed zone, and *D* is the depth to detachment (Fig. 4B)

Depth to the detachment surface (from the stratigraphic level where accommodation began to be generated) is estimated as 2525 m. The width of the stepover is approximated as 1850 m, using the apparent width of the pull-apart basin on the intersecting E-W line. The resulting value of slip *s* = 84 m.

The values of *s* so calculated are subject to a number of errors. The quantities *w* and *D* may be in error by ~10%. More seriously, the geometry of the volume of transtension is assumed to narrow progressively downward to the décollement with the prismatic geometry shown in Fig. 4C, consistent with the interpretation of seismic profile BB' shown in Fig. 2. However, if the volume is assumed to have a constant cross-section, in plan view, down to the basal décollement, the resulting value of *s* would be halved (41 m). Conversely, if the releasing and restraining bends have the geometry of an inverted pyramid, narrowing to a point at the décollement surface, the resulting volume of extension would be reduced by 33%, resulting in a 50% increase in the estimate of *s* to 123 m. A flared, palm-tree geometry would yield an even higher estimate of *s.* The true geometry of the deformed zone is impossible to determine without 3D seismic data. Furthermore, unconsolidated sediments are likely to undergo lateral compaction, resulting in volume loss, during thrusting (36). The stated values of slip, while useful, must therefore be regarded as order-of-magnitude estimates.

Data availability

SEG-Y seismic data are proprietary to Cairn Energy. Images derived from the data are included with annotations in Figs. 2 - 4, and also in uninterpreted form, without vertical exaggeration, in the Supporting Information (SI).

Acknowledgments

We thank John Clayburn and Cairn Energy for their contribution to the project. Schlumberger's Petrel software licenses donated to the University of Alberta assisted data analysis. Participation by J.W.F.W. and L.G. was supported by National Sciences and Engineering Research Council of Canada Discovery Grants. This paper was written whilst Y.N. was a visiting scholar at University of Colorado, Boulder, supported by a CIRES Visiting Fellow Program funded by NOAA agreement NA17OAR4320101. We are grateful for the helpful comments of two anonymous reviewers, Roger Bilham and Peter DeCelles. We acknowledge the use of public geological data from the United States Geological Survey database, accessed from: fttps://catalog.data.gov/dataset/geologic-map-of-south-asia-geo8ag.

References

1. A. Gansser, *Geology of the Himalayas* (Interscience Publishers, 1964).
2. A. Yin, Cenozoic tectonic evolution of the Himalayan orogen as constrained by along-strike variation of structural geometry, exhumation history, and foreland sedimentation. *Earth-Science Reviews* **76**, 1–131 (2006).
3. H. Lyon-Caen, P. Molnar, Gravity anomalies, flexure of the Indian plate, and the structure, support and evolution of the Himalaya and Ganga Basin. *Tectonics* **4**, 513–538 (1985).
4. D. W. Burbank, R. A. Beck, T. Mulder, "The Himalayan foreland basin" in *The Tectonic Evolution of Asia*, A. Yin, T. M. Harrison, Eds. (Cambridge University Press, 1996), pp. 149–188.
5. J. Hirschmiller, *et al.*, What controls the growth of the Himalayan foreland fold-and-thrust belt? *Geology* **42**, 247–250 (2014).
6. R. Soucy La Roche, L. Godin, Inherited Cross-Strike Faults and Oligocene-Early Miocene Segmentation of the Main Himalayan Thrust, West Nepal. *J. Geophys. Res. Solid Earth* **124**, 7429–7444 (2019).
7. W. Zhao, *et al.*, Deep seismic reflection evidence for continental underthrusting beneath southern Tibet. *Nature* **366**, 557–559 (1993).
8. L. D. Brown, *et al.*, Bright Spots, Structure, and Magmatism in Southern Tibet from INDEPTH Seismic Reflection Profiling. *Science* **274**, 1688–1690 (1996).
9. K. D. Nelson, *et al.*, Partially Molten Middle Crust Beneath Southern Tibet: Synthesis of Project INDEPTH Results. *Science* **274**, 1684–1688 (1996).
10. M. L. Hauck, K. D. Nelson, L. D. Brown, W. Zhao, A. R. Ross, Crustal structure of the Himalayan orogen at ~ 90 east longitude from Project INDEPTH deep reflection profiles. *Tectonics* **17**, 481–500 (1998).
11. R. Bilham, "Himalayan earthquakes: a review of historical seismicity and early 21st century slip potential" in *Himalayan Tectonics: A Modern Synthesis*, Geological Society London Special Publications., P. J. Treloar, M. P. Searle, Eds. (The Geological Society, 2019), p. SP483.16.
12. P. G. DeCelles, *et al.*, Neogene foreland basin deposits, erosional unroofing, and the kinematic history of the Himalayan fold-thrust belt, western Nepal. *GSA Bulletin* **110**, 2–21 (1998).
13. Y. Najman, K. Johnson, N. White, G. Oliver, Evolution of the Himalayan foreland basin, NW India. *Basin Research* **16**, 1–24 (2004).
14. P. G. DeCelles, G. E. Gehrels, J. Quade, T. P. Ojha, Eocene-early Miocene foreland basin development and the history of Himalayan thrusting, western and central Nepal. *Tectonics* **17**, 741–765 (1998).
15. P. G. DeCelles, *et al.*, Detrital geochronology and geochemistry of Cretaceous–Early Miocene strata of Nepal: implications for timing and diachroneity of initial Himalayan orogenesis. *Earth and Planetary Science Letters* **227**, 313–330 (2004).
16. L. Godin, L. B. Harris, Tracking basement cross-strike discontinuities in the Indian crust beneath the Himalayan orogen using gravity data – relationship to upper crustal faults. *Geophysical Journal International* **198**, 198–215 (2014).
17. S. Dasgupta, B. Mukhopadhyay, M. Mukhopadhyay, D. R. Nandy, Role of transverse tectonics in the Himalayan collision: Further evidences from two contemporary earthquakes. *J Geol Soc India* **81**, 241–247 (2013).
18. J. Ni, M. Barazangi, Seismotectonics of the Himalayan collision zone: Geometry of the underthrusting Indian plate beneath the Himalaya. *Journal of Geophysical Research: Solid Earth* **89**, 1147–1163 (1984).
19. H. Paul, S. Mitra, S. N. Bhattacharya, G. Suresh, Active transverse faulting within underthrust Indian crust beneath the Sikkim Himalaya. *Geophys J Int* **201**, 1072–1083 (2015).
20. N. P. Rao, *et al.*, The Mw 6.9 Sikkim–Nepal earthquake of September 2011: a perspective for wrench faulting in the Himalayan thrust zone. *Nat Hazards* **77**, 355–366 (2015).

21. L. Godin, R. Soucy La Roche, L. Waffle, L. B. Harris, “Influence of inherited Indian basement faults on the evolution of the Himalayan Orogen” in *Crustal Architecture and Evolution of the Himalaya–Karakoram–Tibet Orogen*, Geological Society of London Special Publication., R. Sharma, I. Villa, S. Kumar, Eds. (2019).
22. L. Seeber, J. G. Armbruster, R. C. Quittmeyer, “Seismicity and continental subduction in the Himalayan arc” in *Geodynamics Series*, H. K. Gupta, F. M. Delany, Eds. (American Geophysical Union, 1981), pp. 215–242.
23. S. Sahu, N. J. Raju, D. Saha, Active tectonics and geomorphology in the Sone-Ganga alluvial tract in mid-Ganga Basin, India. *Quaternary International* **227**, 116–126 (2010).
24. U. M. S. Pradhan, *et al.*, Geological Map of Petroleum Exploration Block - 10: Biratnagar, Eastern Nepal (2006).
25. T. P. Ojha, R. F. Butler, P. G. DeCelles, J. Quade, Magnetic polarity stratigraphy of the Neogene foreland basin deposits of Nepal. *Basin Research* **21**, 61–90 (2009).
26. B. Prasad, B. S. Pundir, Gondwana biostratigraphy of the Purnea Basin (eastern Bihar, India), and its correlation with Rajmahal and Bengal Gondwana basins. *Journal of the Geological Society of India* **90**, 405–427 (2017).
27. G. S. Stockmal, D. Lebel, M. E. McMechan, P. A. MacKay, Structural style and evolution of the triangle zone and external Foothills, southwestern Alberta: Implications for thin-skinned thrust-and-fold belt mechanisms. *Bulletin of Canadian Petroleum Geology* **49**, 472–496 (2001).
28. G. S. Stockmal, A. Slingsby, J. W. F. Waldron, Deformation styles at the Appalachian structural front, western Newfoundland: implications of new industry seismic reflection data. *Canadian Journal of Earth Sciences* **35**, 1299–1306 (1998).
29. R. J. Twiss, E. M. Moores, *Structural Geology* (Freeman, 1992).
30. N. P. Benesh, A. Plesch, J. H. Shaw, Geometry, kinematics, and displacement characteristics of tear-fault systems: An example from the deep-water Niger Delta. *Bulletin* **98**, 465–482 (2014).
31. R. A. Price, E. W. Mountjoy, Banff (East Half) (1972).
32. M. R. Rao, The subsurface geology of the Indo-Gangetic plains. *Journal of the Geological Society of India* **14**, 217–242 (1973).
33. V. Raiverman, Basin geometry, Cenozoic sedimentation and hydrocarbon prospects in north western Himalaya and Indo-Gangetic plains. *Petroleum Asia Journal* **6**, 67–92 (1983).
34. V. Raiverman, M. L. Chugh, A. K. Srivastava, D. N. Prasad, S. K. Das, “Cenozoic Tectonics of the Fold Belt of Himalaya and the Indo-Gangetic Fordeep with Pointers towards Hydrocarbon Prospects” in *Proceedings of the Second Seminar on Petroliferous Basins of India: Himalayan Foothills, Vindhyan and Gondwana Basins, Geoscientific Studies and Hydrocarbon Exploration Techniques*, S. K. Biswas, *et al.*, Eds. (1994), pp. 25–54.
35. S. Calassou, C. Larroque, J. Malavieille, Transfer zones of deformation in thrust wedges: an experimental study. *Tectonophysics* **221**, 325–344 (1993).
36. R. W. H. Butler, D. A. Paton, Evaluating lateral compaction in deepwater fold and thrust belts: How much are we missing from “nature’s sandbox”? *GSAT*, 4–10 (2010).
37. R. V. Almeida, J. Hubbard, L. Liberty, A. Foster, S. N. Sapkota, Seismic imaging of the Main Frontal Thrust in Nepal reveals a shallow décollement and blind thrusting. *Earth and Planetary Science Letters* **494**, 216–225 (2018).
38. S. Ghimire, M. Kasahara, Source process of the Ms=6.6, Udayapur earthquake of Nepal–India border and its tectonic implication. *Journal of Asian Earth Sciences* **31**, 128–138 (2007).
39. T. Ader, *et al.*, Convergence rate across the Nepal Himalaya and interseismic coupling on the Main Himalayan Thrust: Implications for seismic hazard. *Journal of Geophysical Research: Solid Earth* **117** (2012).
40. S. G. Wesnousky, Geological observations on large earthquakes along the Himalayan frontal fault near Kathmandu, Nepal. Earth Planet. Sci. Lett. 457, 366–375. *Earth and Planetary Science Letters* **457**, 366–375.
41. G. Rogers, H. Dragbert, Episodic Tremor and Slip on the Cascadia Subduction Zone: The Chatter of Silent Slip. *Science* **300**, 1942–1943 (2003).
42. T. P. Ojha, *et al.*, Magnetic polarity stratigraphy of the Neogene Siwalik Group at Khutia Khola, far western Nepal. *Geological Society of America Bulletin* **112**, 424–434 (2000).

43. J. Suppe, *Principles of Structural Geology* (Prentice Hall, 1983).
44. J. G. Ramsay, *Folding and Fracturing of Rocks* (McGraw Hill, 1967).
45. B. Goscombe, D. Gray, D. A. Foster, Metamorphic response to collision in the Central Himalayan Orogen. *Gondwana Research* **57**, 191–265 (2018).
46. D. A. Kellett, D. Grujic, New insight into the South Tibetan detachment system: Not a single progressive deformation: South Tibetan Detachment System. *Tectonics* **31**, n/a-n/a (2012).
47. R. Soucy La Roche, L. Godin, J. M. Cottle, D. A. Kellett, Preservation of the Early Evolution of the Himalayan Middle Crust in Foreland Klippen: Insights from the Karnali Klippe, West Nepal. *Tectonics* **37**, 1161–1193 (2018).
48. S. Mohanty, Spatio-temporal evolution of the Satpura Mountain Belt of India: A comparison with the Capricorn Orogen of Western Australia and implication for evolution of the supercontinent Columbia. *Geoscience Frontiers* **3**, 241–267 (2012).
49. S. M. Casshyap, A. Khan, Basin of central India: evidence of pre-Trap doming, rifting and palaeoslope reversal. *Journal of African Earth Sciences* **31**, 65–76 (2000).
50. G. Ekström, M. Nettles, A. M. Dziewoński, The global CMT project 2004–2010: Centroid-moment tensors for 13,017 earthquakes. *Physics of the Earth and Planetary Interiors* **200–201**, 1–9 (2012).
51. A. M. Dziewonski, T.-A. Chou, J. H. Woodhouse, Determination of earthquake source parameters from waveform data for studies of global and regional seismicity. *J. Geophys. Res.* **86**, 2825–2852 (1981).
52. P. Wessel, W. H. F. Smith, R. Scharroo, J. Luis, F. Wobbe, Generic Mapping Tools: Improved Version Released. *Eos, Transactions American Geophysical Union* **94**, 409–410 (2013).

Figures

Figure 1. Location maps. *(A)* Generalized map of the Himalaya showing principal Neogene basins. Imagery ©2019 TerraMetrics, Map data ©2019 used with permission. *(B)* Map of Northern India, Nepal, and adjacent areas, from published sources (2, 21, 45–49) and USGS public data. Approximate traces of basement ridges after Godin & Harris (16). ITSZ: Indus-Tsangpo Suture Zone; STD: South Tibet Detachment; MCT: Main Central Thrust; MBT: Main Boundary Thrust; MFT: Main Frontal Thrust. Focal mechanisms and depths (km) are derived from the Global Centroid Moment Tensor Project (50, 51) shown for seismic events with moment magnitude Mw > 5.5 during the period 1976-2019, plotted with the aid of GMT software (52). Box encloses area of Fig. 4C.

Figure 2. Block 10 area. *(A)* Map of 2D seismic reflection lines superimposed on shaded digital elevation model (DEM) derived from Shuttle Radar and Topography Mission 1-arc-second model; Logarithmic scale, relative to mean sea level. Contours show elevation relative to sea-level of near-top Middle Siwalik elevation surface. Also shown are Biratnagar-1 well, interpreted steep faults 1-6, locations of related contractional and extensional fault-related folds, Main Central Thrust (MCT), Main Boundary Thrust (MBT), Main Frontal Thrust (MFT) and interpreted subsurface slipped area of the outer frontal thrust (Bhadrapur Thrust) between faults 1 and 2 (diagonal shading). ***(B)*** Interpreted seismic profile BB' shown at vertical exaggeration x3, with stratigraphic horizons and steep faults 1-6 marked. Q: Quaternary horizon contoured in Fig. 4. Uninterpreted images of seismic lines are provided in the Supporting Information.

Figure 3. Seismic profiles CC' (10-073-565-2) and DD' (10-78-200) across Bhadrapur high between steep faults 1 and 2 showing interpreted structures at x3 vertically exaggerated (top) and natural scale (bottom). E-G represent deformation zones. OFT = outer frontal thrust system comprising the subhorizontal Bhadrapur Thrust segment and overlying deformation zones. Line locations shown in Fig. 2. Uninterpreted images of seismic lines are provided in the Supporting Information.

Figure 4. Estimation of fault slip. *(A)* Enlargement of seismic profile BB' showing area of structural relief (A_{sr}) and its relationship to slip s. *(B)* Schematic block diagram showing quantities depth (D), width (w) and slip (s) used in estimation of strike-slip motion assuming prismatic volumes of deformation at releasing and restraining bends. Other abbreviations as Fig. 3. *(C)* Schematic structure contour map of a strong peak Quaternary seismic reflection Q (Fig. 2), superimposed on DEM.

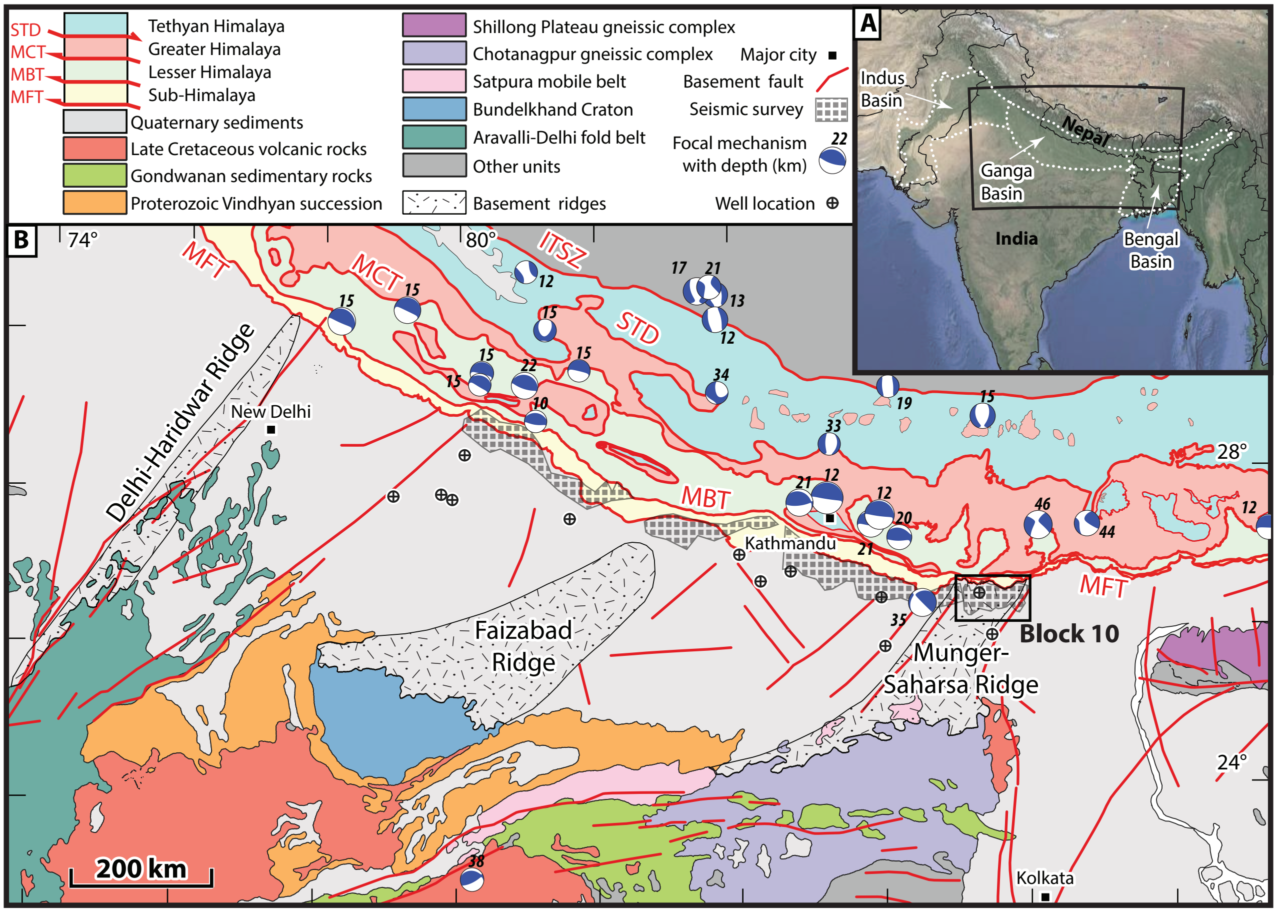

STD
MCT
MBT
MFT
Tethyan Himalaya
Greater Himalaya
Lesser Himalaya
Sub-Himalaya
Quaternary sediments
Late Cretaceous volcanic rocks
Gondwanan sedimentary rocks
Proterozoic Vindhyan succession
Shillong Plateau gneissic complex
Chotanagpur gneissic complex
Satpura mobile belt
Bundelkhand Craton
Aravalli-Delhi fold belt
Other units
Basement ridges
Major city
Basement fault
Seismic survey
Focal mechanism with depth (km)
Well location
A
Indus Basin
Ganga Basin
Nepal
India
Bengal Basin
B
74°
80°
28°
24°
ITSZ
Delhi-Haridwar Ridge
New Delhi
Kathmandu
Faizabad Ridge
Munger-Saharsa Ridge
Block 10
Kolkata
200 km

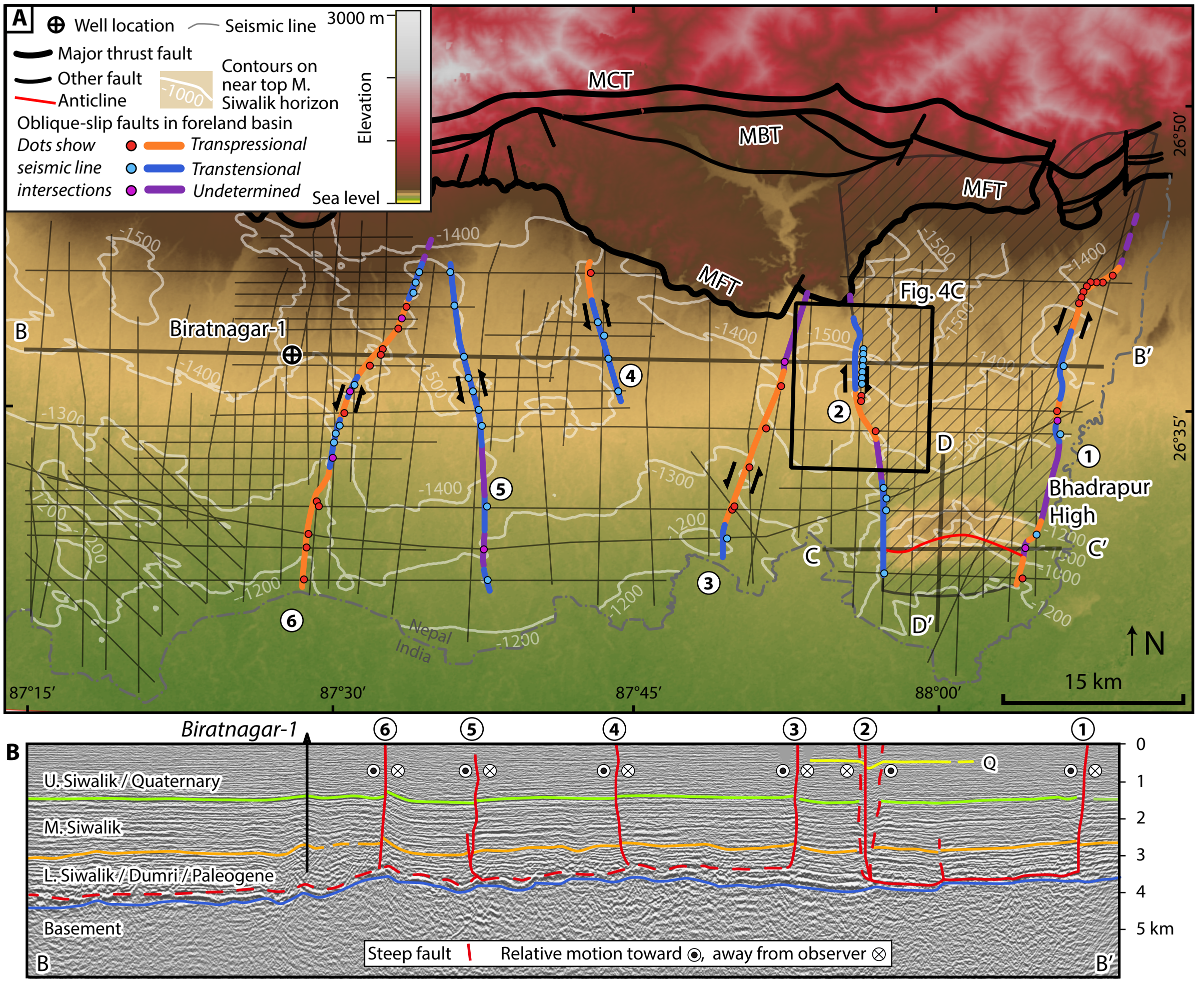

A
Well location
Seismic line
3000 m
Major thrust fault
Other fault
Anticline
Contours on near top M. Siwalik horizon
-1000
Elevation
Sea level
Oblique-slip faults in foreland basin
Dots show seismic line intersections
Transpressional
Transtensional
Undetermined
MCT
MBT
MFT
Fig. 4C
Biratnagar-1
B
B′
C
C′
D
D′
Bhadrapur High
Nepal
India
26°50′
26°35′
87°15′
87°30′
87°45′
88°00′
15 km
N
B
Biratnagar-1
U. Siwalik / Quaternary
M. Siwalik
L. Siwalik / Dumri / Paleogene
Basement
Q
0
1
2
3
4
5 km
Steep fault
Relative motion toward , away from observer

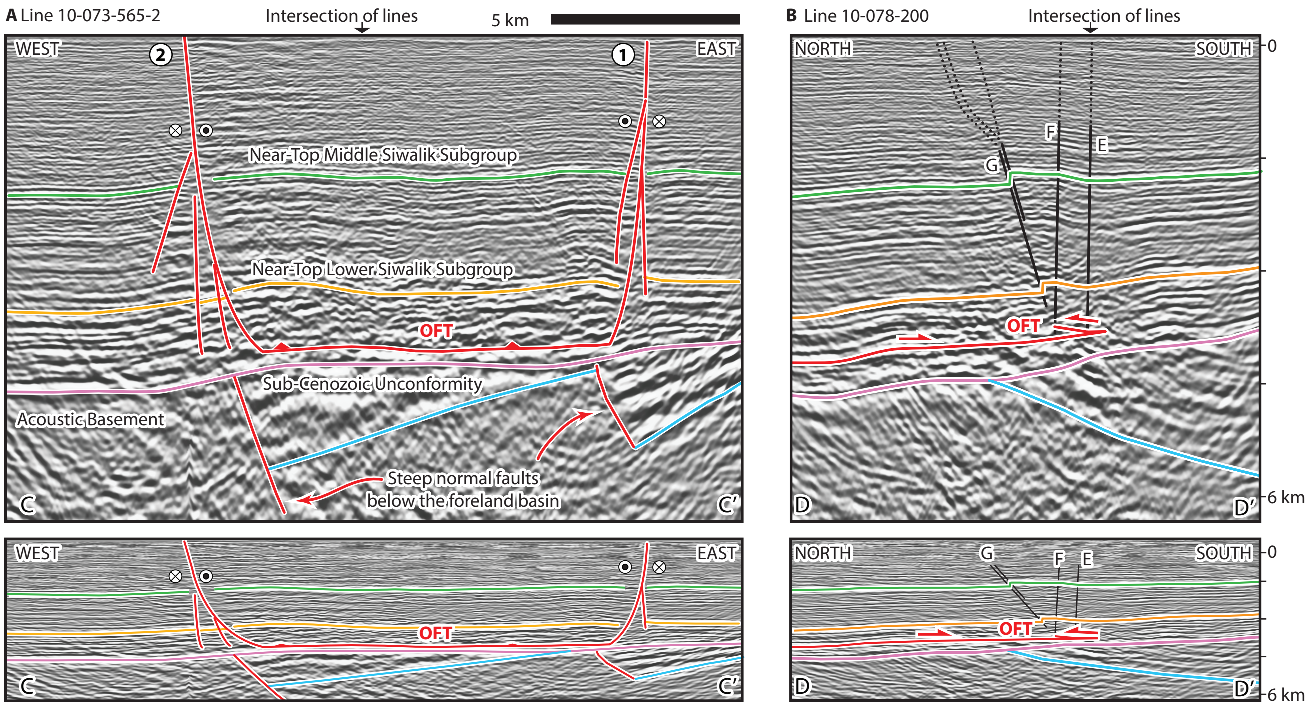
A Line 10-073-565-2
Intersection of lines
5 km
WEST
EAST
2
1
Near-Top Middle Siwalik Subgroup
Near-Top Lower Siwalik Subgroup
OFT
Sub-Cenozoic Unconformity
Acoustic Basement
Steep normal faults
below the foreland basin
C
C′
B Line 10-078-200
Intersection of lines
NORTH
SOUTH
G
F
E
OFT
D
D′
0
6 km

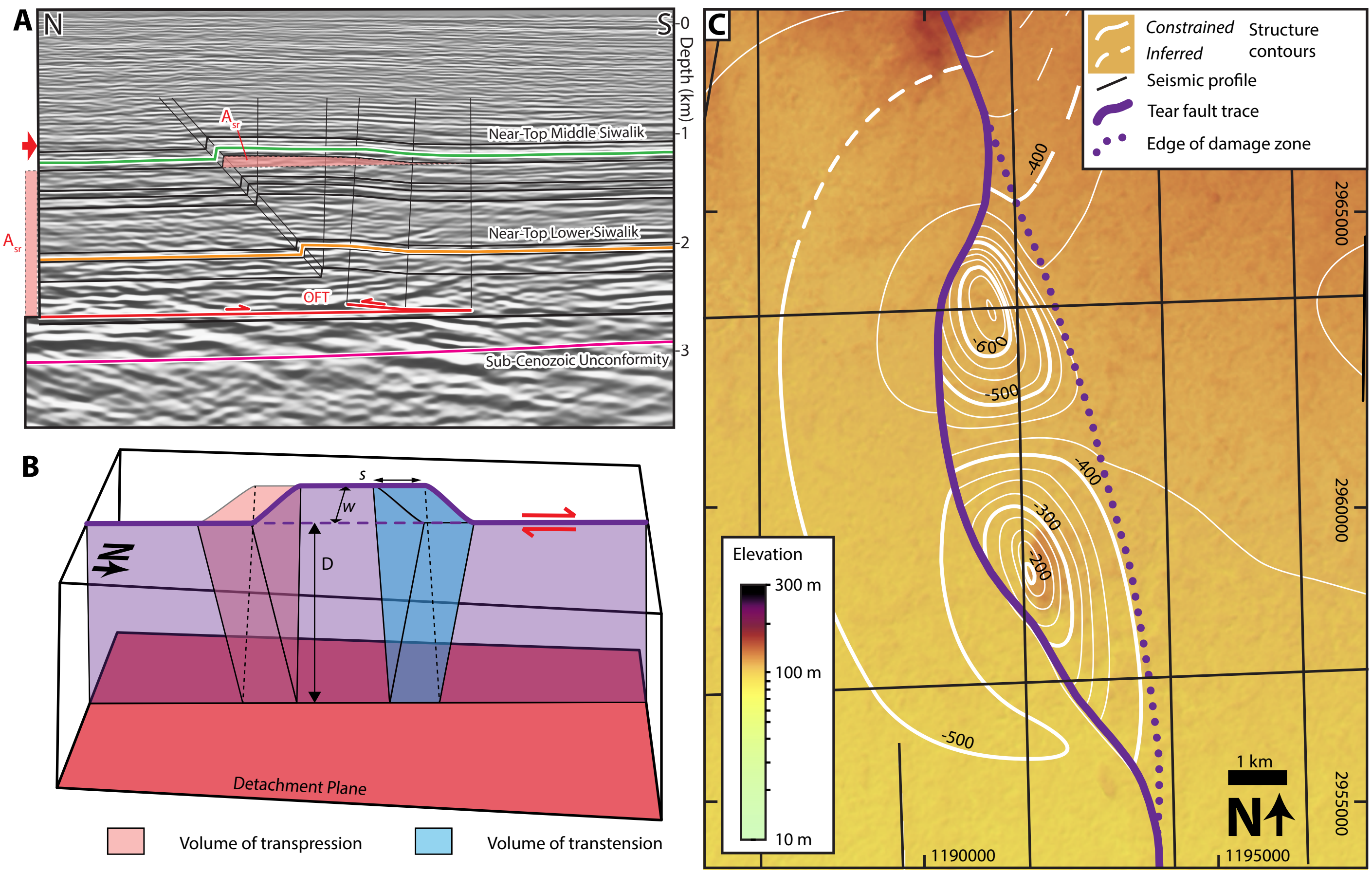
A
N
S
Depth (km)
0
1
2
3
Near-Top Middle Siwalik
Near-Top Lower Siwalik
OFT
Sub-Cenozoic Unconformity
A_{sr}
A_{sr}
B
s
w
D
Detachment Plane
Volume of transpression
Volume of transtension
C
Constrained
Inferred
Structure contours
Seismic profile
Tear fault trace
Edge of damage zone
-400
-600
-500
-400
-300
-200
-500
Elevation
300 m
100 m
10 m
1 km
N
2965000
2960000
2955000
1190000
1195000